

Structure and phase behavior of high-density ice from molecular-dynamics simulations with the ReaxFF potential

Cite as: J. Chem. Phys. **153**, 114501 (2020); <https://doi.org/10.1063/5.0016565>

Submitted: 05 June 2020 . Accepted: 27 August 2020 . Published Online: 16 September 2020

Yuji Adachi, and Kenichiro Koga 



View Online



Export Citation



CrossMark

ARTICLES YOU MAY BE INTERESTED IN

[A fast and high-quality charge model for the next generation general AMBER force field](#)
The Journal of Chemical Physics **153**, 114502 (2020); <https://doi.org/10.1063/5.0019056>

[Free energy barriers from biased molecular dynamics simulations](#)
The Journal of Chemical Physics **153**, 114118 (2020); <https://doi.org/10.1063/5.0020240>

[Crystal imperfections in ice I_h](#)
The Journal of Chemical Physics **153**, 110902 (2020); <https://doi.org/10.1063/5.0019067>



Your Qubits. Measured.

Meet the next generation of quantum analyzers

- Readout for up to 64 qubits
- Operation at up to 8.5 GHz, mixer-calibration-free
- Signal optimization with minimal latency

[Find out more](#)



Structure and phase behavior of high-density ice from molecular-dynamics simulations with the ReaxFF potential

Cite as: *J. Chem. Phys.* **153**, 114501 (2020); doi: [10.1063/5.0016565](https://doi.org/10.1063/5.0016565)

Submitted: 5 June 2020 • Accepted: 27 August 2020 •

Published Online: 16 September 2020



View Online



Export Citation



CrossMark

Yuji Adachi^{1,a)} and Kenichiro Koga^{2,b)} 

AFFILIATIONS

¹Graduate School of Natural Sciences, Okayama University, Okayama 700-8530, Japan

²Department of Chemistry, Okayama University, Okayama 700-8530, Japan

^{a)}Also at: MEC Company Ltd., Hyogo 660-0822, Japan.

^{b)}Author to whom correspondence should be addressed: koga@okayama-u.ac.jp. Also at: Research Institute for Interdisciplinary Science, Okayama University, Okayama 700-8530, Japan.

ABSTRACT

We report a molecular dynamics simulation study of dense ice modeled by the reactive force field (ReaxFF) potential, focusing on the possibility of phase changes between crystalline and plastic phases as observed in earlier simulation studies with rigid water models. It is demonstrated that the present model system exhibits phase transitions, or crossovers, among ice VII and two plastic ices with face-centered cubic (fcc) and body-centered cubic (bcc) lattice structures. The phase diagram derived from the ReaxFF potential is different from those of the rigid water models in that the bcc plastic phase lies on the high-pressure side of ice VII and does the fcc plastic phase on the low-pressure side of ice VII. The phase boundary between the fcc and bcc plastic phases on the pressure, temperature plane extends to the high-temperature region from the triple point of ice VII, fcc plastic, and bcc plastic phases. Proton hopping, i.e., delocalization of a proton, along between two neighboring oxygen atoms in dense ice is observed for the ReaxFF potential but only at pressures and temperatures both much higher than those at which ice VII–plastic ice transitions are observed.

Published under license by AIP Publishing. <https://doi.org/10.1063/5.0016565>

I. INTRODUCTION

A common feature in crystalline ice phases consisting of H₂O molecules is that each molecule has four hydrogen-bonded neighbors. Molecular dynamics (MD) simulation studies, however, reported a possibility of plastic crystal phases in which water molecules freely or frequently rotate at their lattice sites.^{1–5} The simulated plastic ice phases are found to be stable at pressures and temperatures in the domain of ice VII; a schematic phase diagram of dense ice and liquid water is shown in Fig. 1. Takii *et al.*,¹ Aragonés *et al.*,² and Aragonés and Vega³ demonstrated, using common rigid-body models of water, that as the temperature is increased at a fixed pressure, ice VII is transformed into a plastic phase, keeping the body-centered cubic (bcc) lattice, and then into liquid water. It was also noted¹ that a plastic ice phase with the face-centered cubic (fcc) lattice may also be a stable phase depending on the choice

of models. Aragonés and Vega³ reported high-pressure phase diagrams of three common models of water, all of which have both the bcc and fcc plastic ices as stable phases. Structural and dynamical properties of the bcc and fcc plastic ices have been studied in detail.⁶

Although no plastic ice phase is confirmed yet by experiment, some anomalies in ice VII have been reported in several experimental studies. Raman spectroscopy studies found that the pressure-dependent linewidth of the ν_1 OH stretching mode exhibits a minimum around 12 GPa,^{7,8} that the diffusion coefficient of protons in ice VII becomes maximal around 10 GPa,⁹ and that the pressure-dependent Raman modes undergo anomalous changes at 13 GPa–15 GPa;¹⁰ x-ray diffraction studies suggest a structural change from the cubic lattice to a tetragonal structure upon compression between 11 GPa and 14 GPa,^{11,12} and an earlier neutron diffraction study reported a structural change of ice VII to a structure

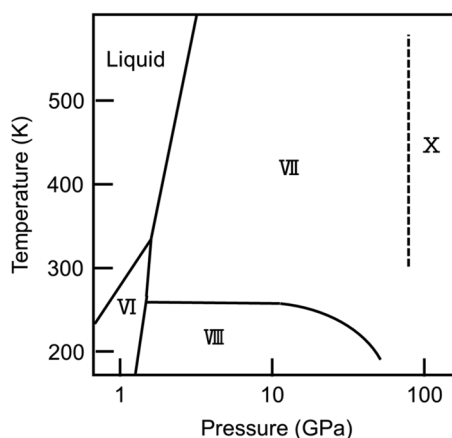


FIG. 1. A schematic phase diagram of high-density water. The numbers VI, VII, VIII, and X indicate crystalline ice phases.

in which deuterons occupy interstitial sites of the oxygen sublattice starting at 13 GPa;¹³ but a recent study finds no evidence to support the interstitial model.¹⁴ A recent study based on a novel nuclear magnetic resonance (NMR) technique shows that the chemical shift of proton changes discontinuously at 20 GPa and 75 GPa at room temperature, suggesting that the first transition is between two domains of ice VII with high-barrier and low-barrier hydrogen bonds.¹⁵ In short, anomalous structural and dynamical behaviors in ice VII have been observed at pressures much lower than that of the VII–X phase transition, but the origin of the anomalies remains unclear.

While rigid-body models of water exhibit phase transitions to plastic ice at high pressures,^{1–6,16} water simulated by *ab initio* MD simulation undergoes structural changes from ice VII, where the proton density distribution between a given pair of neighboring oxygen atoms is unimodal, to a phase called ice VII', where the proton distribution is bimodal.^{17–22} The bimodal distribution results from proton hopping, not from rotational motion of molecules, and so ice VII' is not a plastic solid. The recent high-pressure NMR study reports evidence for quantum-mechanical tunneling of protons in ice VII.¹⁵ Until recently, first-principles MD studies had not provided evidence to support plastic ice; however, Hernandez and Caracas for the first time showed the appearance of bcc plastic ice.²³

Here, we report the high-pressure phase behavior of water obtained by MD simulations with a reactive force field (ReaxFF). Since its invention,²⁴ the ReaxFF has developed into a major atomistic force field and has been applied to a wide variety of reactive systems.²⁵ The reactive MD simulation technique is atomistic in the sense that molecules, now H₂O, are not predefined but spontaneously form from the constituent atoms. Thus, the reactive force field is potentially applicable to wider ranges of pressures and temperatures where molecular structure may be deformed or different molecular species may form. Furthermore, one can simulate with this force field a system consisting of thousands of atoms with a reasonable computational cost, which is an advantage over *ab initio*

MD simulation when examining phase transitions in a macroscopic system.

We will see that plastic ice spontaneously forms in the reactive force field as it does in the rigid-body models. However, the phase diagram deduced from the present simulation is different from those of the classical models or that implied by *ab initio* MD simulation.²³

Our paper is organized as follows. In Sec. II, we describe the model system and the method of simulation; in Sec. III, we present simulation results, structural and dynamics analyses, and a phase diagram of this water model; Sec. IV is devoted to conclusions and outlook on further studies.

II. COMPUTATIONAL DETAILS

We performed NpT and NVT MD simulations of water using the reactive force field ReaxFF. This method assumes the potential energy of a system consisting of atoms (H and O atoms with the ratio 2:1 in the present study) at given positions to be the sum of the bond energy E_{bond} , the energy penalty E_{over} for forming extra bonds, the three-body (valence angle) energy E_{angle} , the four-body (torsional angle) energy E_{tor} , the van der Waals and Coulomb energies E_{vdW} and E_C , and the specific energy E_{spec} required to account for specific interactions such as the hydrogen bond. The ReaxFF parameters for H and O atoms employed in the present study are those listed in the supplementary material in Ref. 26. The ReaxFF potential has been employed for MD simulations of bulk, interfacial, and confined water.^{27–30} The molecular structure of H₂O in bulk water is very close to that determined by experiment, the dipole moment in bulk water is less than the experimental value, and both structural and dynamical properties of bulk water are in fair agreement with the experimental results.²⁷ Structures and phase behaviors of water confined in carbon nanotubes and water between graphene layers, which were found in earlier simulation studies^{31–33} and later confirmed by experiment,^{34,35} are also well reproduced by the MD simulations with the ReaxFF potential.^{28–30} Given the validity of ReaxFF for simulating water under ambient as well as extreme conditions, it is possible that the flexible, reactive force field is applicable to dense ice and liquid water under high-pressure and/or high-temperature conditions where rigid-body models of water become unreliable.

The model system consists of 1024 oxygen atoms and 2048 hydrogen atoms. All the MD simulations were implemented by the large-scale atomic/molecular massively parallel simulator (LAMMPS,³⁶ 17 November 2016 version). The temperature T and the pressure p were fixed by the Nosé–Hoover thermostat and barostat: the simulation cell is a rectangular parallelepiped, subject to periodic boundary conditions, with the ratios of three dimensions not being fixed. In the case of the NVT MD simulation, a cubic simulation cell was employed. The oxygen atoms were initially arranged to form ice VIII with the lattice constant $a = b = 3.1 \text{ \AA}$ and $c = 3.244 \text{ \AA}$, and the hydrogen atoms are placed at midpoints between oxygen atoms in each sublattice of ice VII. An equilibration run was carried out for 10 ps at 8 GPa and 100 K, followed by an isobaric heating process ending at 300 K, and then, we found that the structure of ice VII, having a bcc lattice and a proton-disordered configuration, formed spontaneously during that process. It was also confirmed that the same structure of ice VII, with a different

proton-disorder arrangement, was obtained starting from the structure of ice X. Thermodynamic-state points examined in the present study range in temperature from 300 K to 600 K and in pressure from 4 GPa to 42 GPa. The temperature and pressure were changed stepwise, respectively, by 5 K–10 K and by 0.01 GPa–0.1 GPa. As we will see below, in this range of the thermodynamic states, crystal-plastic, crystal-crystal, and solid-liquid spontaneous phase changes were observed.

III. RESULTS AND DISCUSSION

A. Appearance of plastic ice: Dynamics

One of the features of a plastic crystal of small molecules is rotational motions of the molecules. Thus, to examine the existence of plastic crystal phases of H_2O modeled by the ReaxFF potentials, we first evaluate reorientation dynamics of molecules in dense ice at several pressures and temperatures. Figure 2 shows the time-correlation

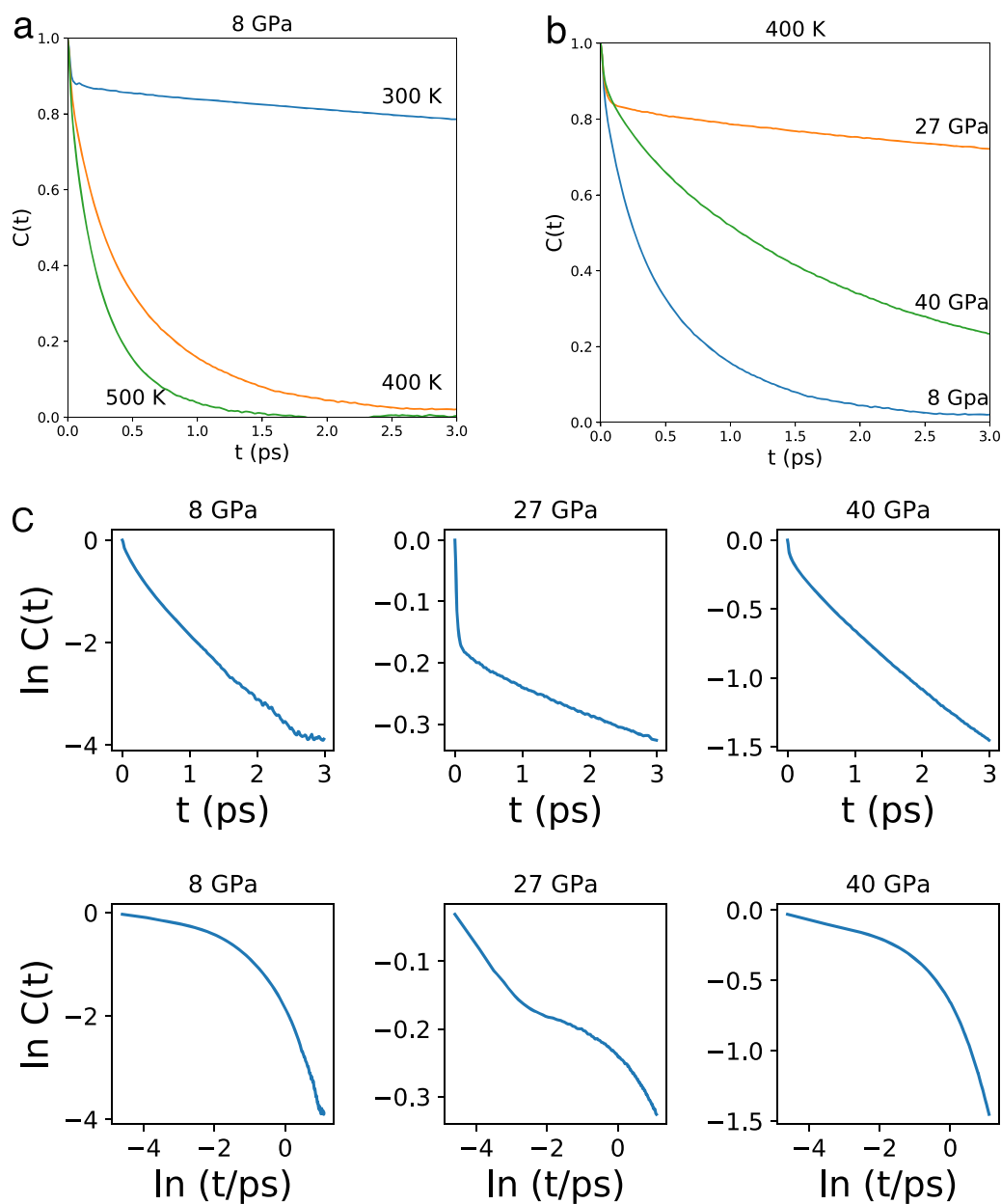


FIG. 2. The reorientational correlation function $C(t)$ of H_2O molecules in high-density ice: (a) 300 K, 400 K, and 500 K at 8 GPa; (b) 8 GPa, 27 GPa, and 40 GPa at 400 K; and (c) semi-log (upper row) and log-log (second row) plots of $C(t)$ in (b).

function of the unit vector $\mathbf{u}(t)$ along the dipole moment of a water molecule, or the reorientational correlation function, defined by

$$C(t) = \langle \mathbf{u}(t) \cdot \mathbf{u}(0) \rangle,$$

where the average is taken over all molecules and over the time origins. The dipole moment of each molecule is calculated from the instantaneous positions of its H and O atoms assuming charge neutrality in the molecule and charge symmetry for two H atoms.

Shown in Fig. 2(a) are $C(t)$ at $T = 300$ K, 400 K, 500 K, all under 8 GPa. The reorientational correlation decays rapidly and vanishes within 3 ps at 400 K and 500 K, indicating that water molecules at lattice sites freely rotate with some characteristic time shorter than 3 ps. At 300 K, however, the correlation function decays to ~ 0.8 in 3 ps, meaning that the water molecules do not rotate frequently.

Plotted in Fig. 2(b) are $C(t)$ for three different pressures, 8 GPa, 27 GPa, and 40 GPa, all at 400 K. The reorientational correlation decays very rapidly at 8 GPa, and it decays considerably within 3 ps at 40 GPa [$C(t) \sim 0.2$ at 3 ps], but the correlation does not disappear at 27 GPa. Thus, the pressure dependence of $C(t)$ is non-monotonic: water molecules rotate more or less freely at the low and high pressures, but they do not at the medium pressure. This result implies the reentrant appearance of plastic crystal phases. It is clear from semi-log plots of $C(t)$ in Fig. 2(c) that the reorientational correlations at 8 GPa and 40 GPa decays exponentially with a characteristic time τ : $C(t) = \exp(-t/\tau)$. On the other hand, as seen from the semi-log and log-log plots, the reorientational correlation at 27 GPa and 400 K shows a power-law decay $C(t) \sim t^{-\alpha}$ in a sub-picosecond time scale and an exponential decay in a longer time scale. This type of decay in the reorientational correlation function of water molecules indicates that hydrogen-bond rearrangement occurs only occasionally in a short period and otherwise water molecules do not change hydrogen-bonding partners.³⁷

Table I lists the characteristic time τ of the exponential decay of the reorientational correlation function $C(t)$ at selected temperatures and pressures: τ ranges 0.35 ps–9 ps. Considering the fact that the average lifetime of hydrogen bonds in liquid water at room temperature is 2 ps–3 ps,³⁸ ice with the finite values of τ may be considered a “liquid” with regards to rotational motion, i.e., a plastic solid. Blank cells in Table I are those cases in which $C(t)$ does not decay appreciably within 3 ps or decays in a power-law fashion in a sub-picosecond time scale.

To check the dynamical properties of the ReaxFF liquid water at high pressures, we calculated translational and rotational diffusion coefficients, D_T and D_R ,³⁹ of water molecules under 0.1 GPa, 1 GPa, 2 GPa, and 3 GPa at 400 K. It is found that D_T decreases with increasing pressure, while D_R is nearly constant. This trend is

TABLE I. The characteristic time τ (ps) of the exponential decay for the reorientational correlation function $C(t)$ as obtained from fitting in the interval 0.2 ps–1.2 ps. The blank cells correspond to non-plastic states in which $C(t)$ does not decay to values less than 0.7 in 3 ps.

	300 K	400 K	500 K
8 Gpa	...	0.66	0.35
27 Gpa	0.58
40 Gpa	8.78	2.02	1.00

qualitatively the same as the experimental results obtained by Bove *et al.*⁴⁰ However, the diffusion coefficients obtained from the ReaxFF potential are consistently larger than the corresponding experimental data. The values of D_T and D_R are given in the [supplementary material](#).

B. Appearance of plastic ice: Structure

Unlike classical force field models, the ReaxFF model treats each molecule as interacting atoms, and so molecules may dissociate and rearrange covalent bonds. Therefore, in addition to the possibility of rotational motions of H₂O in dense ice, a proton between two neighboring oxygen atoms may hop from one potential well to another exchanging its covalent- and hydrogen-bonding oxygen atoms. Such proton hopping motions are observed in *ab initio* MD simulations.²³

Anticipating the two possibilities, we look at the distribution of relative coordinates of a proton during $\Delta t = 3$ ps from a reference time t_0 . Shown in Fig. 3(a) is the coordinate system, in which the origin is taken to be the position of the oxygen atom closest to the proton in question and the x-axis is defined by the position of the second nearest oxygen atom. The coordinate system is defined at $t = t_0$ and is kept fixed over Δt , while the positions of the two oxygen atoms fluctuate. The coordinates x_H, y_H, z_H of the proton evolve during the interval Δt . Figure 3(b) shows the distributions f_x of x_H during Δt , which is averaged over the choices of t_0 with equal intervals of 0.1 ps and over all the protons in the system. The function $f_x(x)$ would have a single peak at around 1 Å if the covalent bond O–H is intact and if the hydrogen bond along the x-direction is kept during Δt ; $f_x(x)$ would have double peaks, one at around 1 Å and another at around 1 Å from the other oxygen atom, if the proton hops between two potential wells corresponding to O–H···O and O···H–O, where ··· denotes hydrogen bonds; $f_x(x)$ would show a broad distribution with a tail extending over the range $x < 0$ if the molecule rotates frequently during Δt . It is seen in Fig. 3(b) that $f_x(x)$ does not have double peaks in the range $x > 0$, confirming that no proton hopping occurs during Δt at any of the nine states examined here. In three cases, (300 K, 8 GPa), (300 K, 27 GPa), and (400 K, 27 GPa), $f_x(x)$ has a sharp, single peak, indicating that these solids are crystalline ice. In four out of the remaining six cases, (400 K, 8 GPa), (500 K, 8 GPa), (500 K, 27 GPa), and (500 K, 40 GPa), $f_x(x)$ shows broad distributions of x_H extending over the range $-1 < x < 1$, while in the other two cases, (300 K, 40 GPa) and (400 K, 40 GPa), the distributions have tails extending over $x < 0$, but they are less broad than the former cases. It is confirmed that in the above six cases, the reorientational correlation function $C(t)$ decays exponentially rapidly as we saw in Fig. 2, suggesting that these solids are plastic ice.

Figure 3(c) shows distributions f_{yz} of a proton projected on the y, z plane. In the three cases, (300 K, 8 GPa), (300 K, 27 GPa), and (400 K, 27 GPa), the distributions are sharper than in the others, having peaks at the center. In the cases (400 K, 8 GPa) and (500 K, 8 GPa), the distributions are very broad, indicating that molecules are rotating nearly freely. Finally, in the three cases of 40 GPa, there appear broad, annular distributions, which are distinct from broad distributions at 8 GPa. The ring-shaped distributions in f_{yz} together with the corresponding distributions $f_x(x)$ in Fig. 3(b) indicate that O–H···O atoms are less likely to be colinear

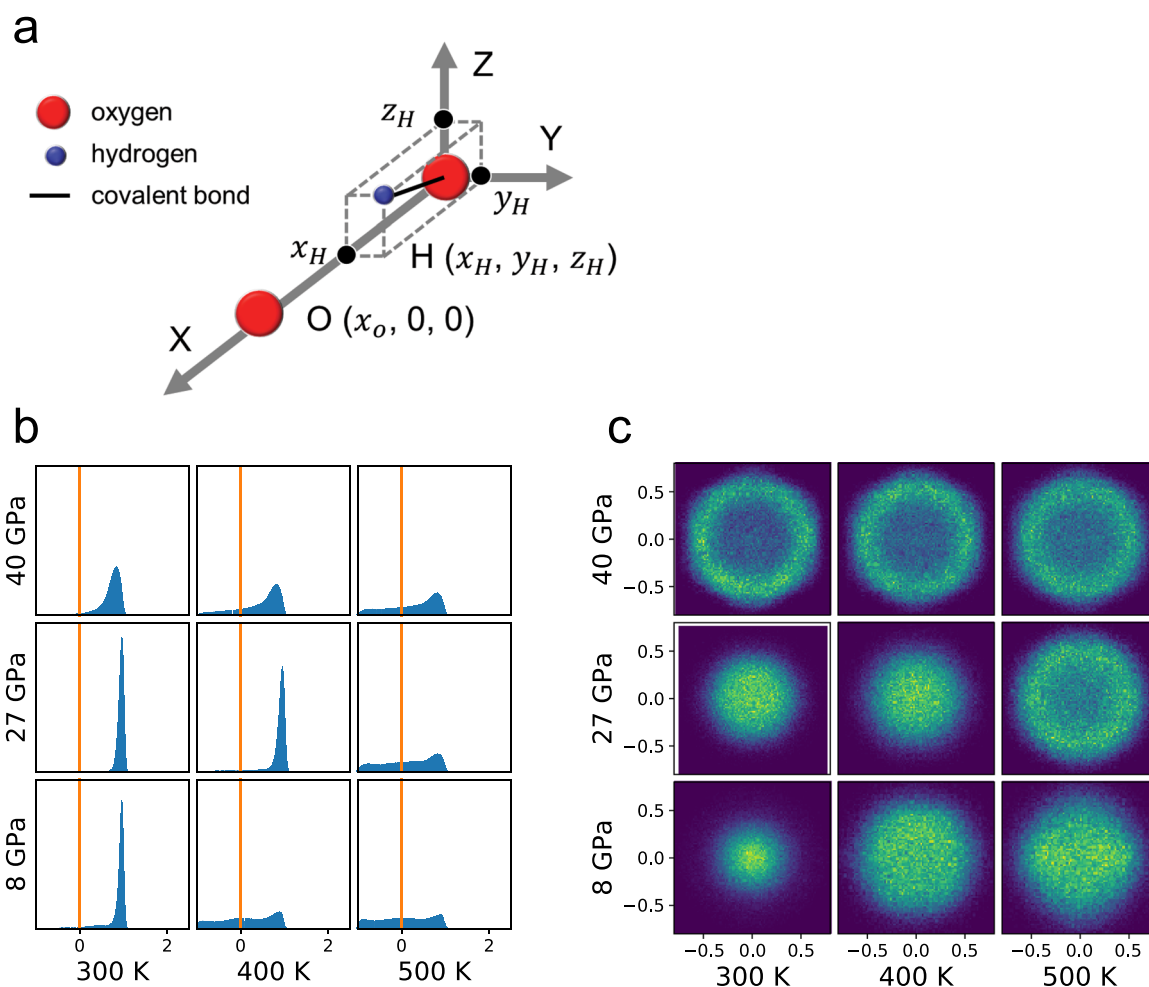


FIG. 3. Distributions of a proton between two neighboring oxygen atoms in a time interval $\Delta t = 3$ ps starting from a reference time t_0 . (a) The coordinate system defined at t_0 ; (b) the distributions f_x of the x -coordinate x_H ; (c) the distributions f_{yz} of the y - and z -coordinates y_H and z_H on the yz plane. The lighter the tone, the larger the distribution.

and water molecules undergo precession and occasionally rotate to change their hydrogen-bonding partners.

Earlier simulation studies of classical models of water have shown that there are two stable plastic ice phases, the one with body-centered cubic (bcc) and the other with face-centered cubic (fcc) lattice structures.^{1,3} The two phases with the bcc and fcc lattice may transform to each other via a martensitic phase transition, just by scaling the z coordinate of the bcc lattice in Fig. 4(a).³

Now, we examine the lattice structures of plastic ice given by the reactive force field (ReaxFF). Figure 4 shows spatial distributions of oxygen atoms that are the nearest neighbors of each oxygen atom for the same nine states as in Fig. 3. The xyz coordinate systems for the bcc and fcc lattices are now defined in Fig. 4(a). Figure 4(b) shows the projection of the distribution on the x, y plane, and Fig. 4(c) shows that on the x, z plane. Among the nine states, three states (300 K, 8 GPa), (300 K, 27 GPa), and (400 K, 27 GPa), correspond to those of

ice VII, and the other six states correspond to those of plastic ice. In each of the three cases of ice VII, there appear four spots in the projection on the x, y and x, z planes, reflecting eight nearest neighbors' characteristic of the bcc lattice. In four cases of plastic ice, (500 K, 27 GPa), (300 K, 40 GPa), (400 K, 40 GPa), and (500 K, 40 GPa), there are four spots as in the cases of ice VII: they have the bcc lattice. However, in the other two cases, (400 K, 8 GPa) and (500 K, 8 GPa), of plastic ice, there are eight spots in the projection on the x, y plane and seven spots in the projection on the x, z plane. This reflects their fcc lattice structure. We have also confirmed that the relative dimensions of the simulation cell at two cases are consistent with the fcc and bcc lattices.

The oxygen–oxygen radial distribution functions $g(r)$ at 500 K, 27 GPa and 500 K, 8 GPa are shown in the [supplementary material](#). The resulting $g(r)$ at 27 GPa and 8 GPa are, respectively, similar to those of the bcc and fcc plastic crystals obtained for the TIP4P/2005 potential.³

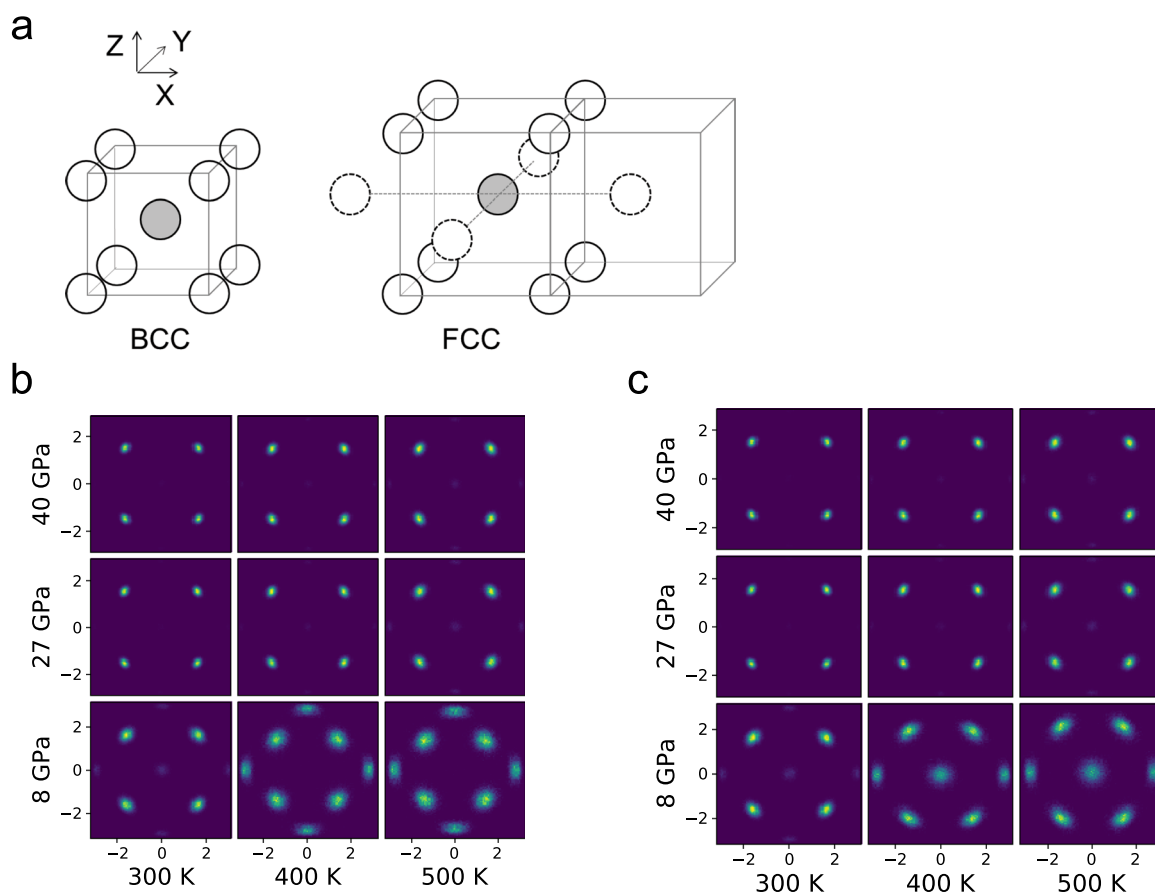


FIG. 4. Density distributions of the nearest neighbor oxygen atoms from each central oxygen atom in high-density ice at nine states: (a) the bcc and fcc lattices of oxygen atoms with the mutual orientations between which a martensitic phase transformation may occur.³ The distributions on (b) the x, y plane and (c) the x, z plane in the coordinate system in (a).

Note that the fcc plastic crystal phase lies at lower pressures (e.g., 8 GPa) than ice VII and the bcc plastic phase, which means that the fcc plastic ice is less dense than ice VII and the bcc plastic ice at the same temperature. In the case of TIP4P/2005 water, the fcc plastic ice is denser than the bcc plastic ice.³

C. Phase behavior

Having confirmed that fcc and bcc plastic ices both form spontaneously under their respective pressure, temperature conditions in the reactive force field ReaxFF, we will now examine phase changes between ice VII and a plastic crystal phase and between the two plastic crystal phases. In Fig. 5(a), density variations upon compression and decompression between 8 GPa and 20 GPa at 500 K are shown. Upon compression starting from 8 GPa, the density increases continuously until a discontinuous jump occurs at a pressure between 18 GPa and 19 GPa where the bcc plastic ice forms spontaneously from the fcc plastic phase. Upon decompression, the density decreases continuously forming a hysteresis loop up to a pressure between 9 GPa and 10 GPa, where the bcc to fcc plastic phase change occurs, and then, the density follows the same path as compression.

Figure 5(b) shows variations of the density, enthalpy, and potential energy in the low, medium, and high pressure ranges. In the pressure range of the hysteresis loop, differences in the potential energy ΔU , the pressure-volume term $p\Delta V$, and the enthalpy ΔH between the fcc and bcc plastic ices are evaluated, as listed in Table II, where ΔX means $X_{\text{fcc}} - X_{\text{bcc}}$. The potential energy of the fcc plastic ice is lower than that of the bcc plastic ice at any of the three pressures, the difference being smaller at higher pressures. The molar volume of the fcc plastic ice is larger than that of the bcc plastic ice at each pressure as noted above. Furthermore, another counter-intuitive fact is that the molar volume difference $\Delta V (>0)$ increases with increasing pressure, and as a consequence, the pressure-volume term $p\Delta V$ increases more rapidly than linearly with p . Because of $p\Delta V$, the enthalpy difference $\Delta H = \Delta U + p\Delta V$ changes its sign (from negative to positive) with increasing pressure in this range. This, in turn, means that the slope dp/dT of the phase boundary between the fcc and bcc plastic ices may be positive or negative, depending on the equilibrium pressure in the hysteresis range. We can, however, estimate a magnitude of the slope. With ΔH (or ΔU) and $p\Delta V$, the dimensionless slope $(T/p)(dp/dT)$ of the phase

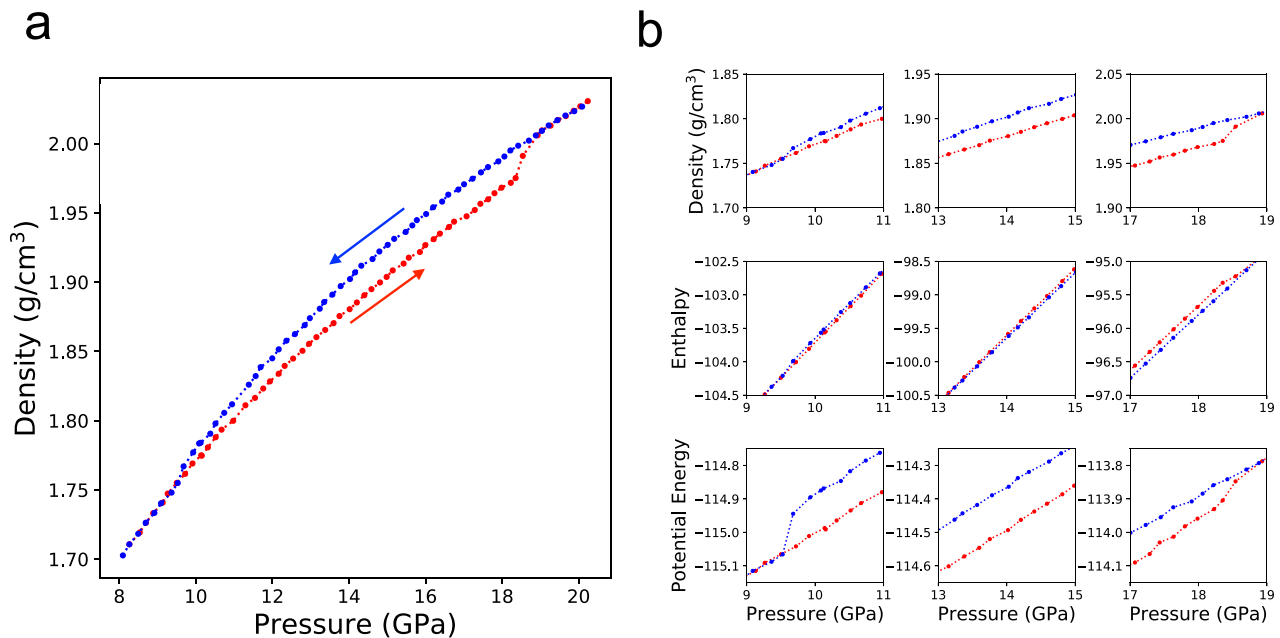


FIG. 5. Isothermal variations of density, enthalpy, and potential energy with increasing and decreasing pressure between 8 GPa and 20 GPa at 500 K. The low- and high-density phases at any given pressure in the hysteresis interval are, respectively, the bcc and fcc plastic ices. (a) Density variations. (b) Density, enthalpy (configurational), and potential energy variations in the low, medium, and high pressure ranges. Blue and red colors indicate data points obtained upon decreasing and increasing pressure.

boundary is given by a Clapeyron equation,

$$\frac{T}{p} \frac{dp}{dT} = \frac{\Delta H}{p\Delta V} = 1 + \frac{\Delta U}{p\Delta V}. \quad (1)$$

We have evaluated $(T/p)(dp/dT)$ using the values of p , ΔU , and ΔV in Table II and listed the values in the same table. We find that the magnitudes are rather small: $|(T/p)(dp/dT)| < 1.3$ or equivalently $|dp/dT| < 0.03$ GPa/K.

Figure 6 illustrates crystalline ice-plastic ice phase transitions as isobaric and isothermal density variations. Figure 6(a) shows isobaric density variations upon heating from 200 K to 400 K at 8 GPa, which include density jumps associated with two phase transitions. One is a transition from ice VIII to VII, which is accompanied by a small increase in density. The other is the ice VII-to-fcc plastic phase

transition accompanied by a large decrease in density. Figure 6(b) shows density variations upon compression and decompression at 300 K. The solid phase on the low-pressure side is ice VII, and the one on the high-pressure side is bcc plastic ice.

As we have seen above, in the ReaxFF water model, the fcc plastic phase is less dense than ice VII and the bcc plastic phase at respective phase boundaries. Then, the O–O distance d_{OO} between neighboring oxygen atoms must increase upon a transition from a bcc phase (ice VII or plastic) to the fcc plastic phase. It is interesting to see how the O–O distance d_{OO} between neighboring oxygen atoms changes upon the transition between fcc and bcc plastic ice phases and the transition between ice VII and fcc plastic ice phases. Assuming the equilibrium pressure to be 14 GPa at 500 K (see Fig. 5), one finds that d_{OO} for the bcc plastic crystal is 2.73 Å, while d_{OO} for the fcc plastic crystal is 2.82 Å. In the case of the transition between ice VII and fcc plastic ice at 320 K and 8 GPa [see Fig. 6(a)], d_{OO} for ice VII is 2.79 Å, while d_{OO} for fcc plastic ice is 2.89 Å. Thus, the above cases illustrate that d_{OO} for fcc plastic ice is three or 4% longer than those for ice VII or bcc plastic ice.

Table III summarizes the phase changes that have been observed during isobaric and isothermal processes in the simulations. Some of the temperatures and pressures at which the spontaneous phase changes are observed may not be close to those at phase equilibrium and may be close to those of the stability limits of mother phases. Hysteresis is observed for the fcc–bcc plastic phase changes on the isothermal paths at 500 K and 600 K and for the VII–bcc plastic phase change on the isothermal path at 300 K.

TABLE II. Differences in the potential energy ΔU (kJ/mol), the molar volume ΔV (cm^3/mol), the pressure-volume term $p\Delta V$ (kJ/mol), and the enthalpy ΔH (kJ/mol) between the fcc and bcc plastic ices at three pressures in the hysteresis loop, where ΔX are defined as $X_{\text{fcc}} - X_{\text{bcc}}$. $(T/p)(dp/dT)$ are the dimensionless slope of the phase boundary evaluated by Eq. (1). The temperature is fixed at 500 K.

P	ΔU	ΔV	$p\Delta V$	ΔH	$\frac{T}{p} \frac{dp}{dT}$
9.9 GPa	−1.04	0.046	0.46	−0.59	−1.29
14.0 GPa	−1.17	0.110	1.54	0.37	0.24
18.2 GPa	−0.64	0.107	1.95	1.31	0.67

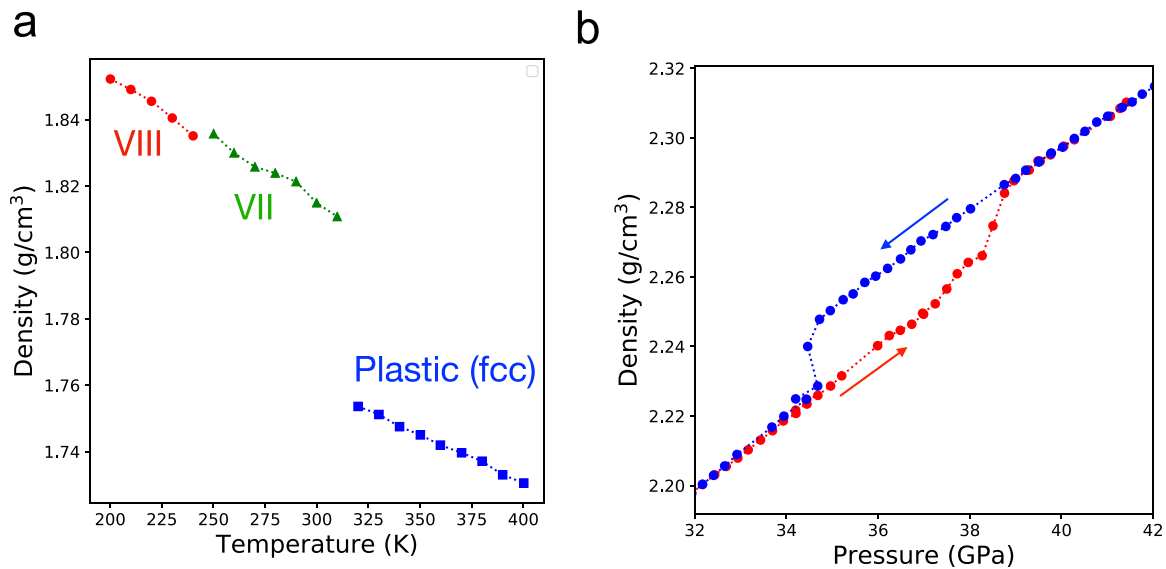


FIG. 6. Density variations associated with VII–VII, VII–fcc plastic, and VII–bcc plastic phase transitions. (a) Density vs temperature at 8 GPa. (b) Density vs pressure at 300 K. Blue and red colors indicate the data points obtained upon decreasing and increasing pressure.

D. Phase diagram

Shown in Fig. 7 is a phase diagram of H₂O derived from our ReaxFF MD simulations. The ice phase with the solid–fluid phase boundary in this temperature range is the fcc plastic crystal: the melting curve has a positive slope, indicating that the fcc plastic ice is denser than the liquid in equilibrium. The fcc plastic phase has a phase boundary with ice VII at temperatures lower than ~410 K; it also has a phase boundary with bcc plastic ice at temperatures higher than ~410 K. The bcc plastic phase lies on the high-pressure side of

the phase boundary with the fcc plastic phase. The fcc–bcc phase boundary is nearly parallel to the temperature axis in the ranges of pressure and temperature in Fig. 7: the estimated slope of the phase boundary is listed in Table II. The triple point of ice VII, fcc plastic, and bcc plastic phases is located around 10 GPa and 410 K. Starting from the triple point, the VII–bcc phase boundary extends toward a higher pressure region, and that phase boundary has a point of maximum temperature, where ice VII and bcc plastic ice have the same density. At pressures above the point of maximum temperature, the bcc plastic ice is denser than ice VII.

The phase diagram of H₂O obtained from our ReaxFF MD simulations has both similarities and differences as compared with the

TABLE III. The phase changes observed in the ReaxFF MD simulations of H₂O.

Fixed T or p	Range of T or p	Phase change
300 K	6 GPa–3 GPa	fcc → liquid at 3.8 GPa
300 K	32 GPa–42 GPa	VII → bcc at 38 GPa
300 K	42 GPa–32 GPa	bcc → VII at 35 GPa
400 K	8 GPa–4 GPa	fcc → liquid at 4.4 GPa
450 K	8 GPa–20 GPa	fcc → bcc at 17 GPa
500 K	8 GPa–20 GPa	fcc → bcc at 18.5 GPa
500 K	20 GPa–8 GPa	bcc → fcc at 9.5 GPa
600 K	8 GPa–20 GPa	fcc → bcc at 19.2 GPa
600 K	20 GPa–8 GPa	bcc → fcc at 9.5 GPa
600 K	8 GPa–4 GPa	fcc → liquid at 6.0 GPa
8 GPa	300 K–400 K	VII → fcc at 320 K
8 GPa	700 K–800 K	fcc → liquid at 750 K
14 GPa	350 K–450 K	VII → bcc at 410 K
18 GPa	400 K–500 K	VII → bcc at 440 K
27 GPa	400 K–500 K	VII → bcc at 430 K
30 GPa	400 K–500 K	VII → bcc at 420 K

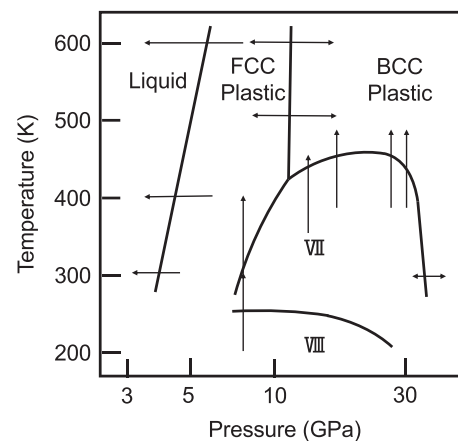


FIG. 7. Phase diagram of high-pressure water obtained from the MD simulations with the ReaxFF potential.

phase diagrams for rigid-molecule models of water.^{3,5} In agreement with the simulation results for rigid-molecule models, the ReaxFF model gives plastic ice as a stable phase being in a part of the region experimentally assigned to ice VII and having a melting line. The ReaxFF model gives both fcc and bcc plastic ice phases as do the TIP4P/2005, TIP4P, and SPC/E models.³ In the phase diagrams of TIP4P/2005 and SPC/E models, the fcc plastic phase occupies a large region on the high-pressure, high-temperature side of the region of ice VII while the bcc plastic ice phase exists marginally in a low-pressure region bounded by the three boundaries with ice VII, the fcc plastic, and liquid water.³ The notable difference from the phase diagrams for the rigid-molecule models is that now the fcc plastic phase exists in the low-pressure region and the bcc plastic phase in the high-pressure region. As remarked above, the fcc plastic phase is less dense than ice VII and than the bcc plastic phase at the respective phase boundaries. Noting that the intermolecular interactions are by far more complex than those of simple liquids, it is not impossible that a solid phase with the fcc lattice is less dense than solid phases with the bcc lattice at their phase boundary. In fact, there is in the phase diagram constructed from *ab initio* calculation a phase boundary between two superionic ice phases along which the fcc phase is less dense than the bcc phase.⁴¹ The phase diagrams of rigid water models and the ReaxFF model and the one obtained from *ab initio* calculation suggest that the relative stability of bcc over fcc dense ice is sufficiently small that it could be reversed by the choice of force field parameters, methodologies, or other computational details. However, it is beyond the scope of the present study to identify the microscopic mechanisms causing those discrepancies.

There are few *ab initio* MD simulation studies examining the existence of a plastic ice phase. In 2018, Hernandez and Caracas reported the first evidence of plastic ice as obtained from *NVT*-ensemble *ab initio* simulations and proposed a phase diagram including the plastic phase.²³ The plastic ice phase is found to exist in a lower-pressure part of the currently accepted domain of ice VII, which is in agreement with the classical simulation result³ and with the present ReaxFF simulation result. At higher pressures, however, the plastic phase is no longer observed. Instead, the *ab initio* simulations found a solid phase called ice VII' in which the density distribution of a proton between two neighboring oxygen atoms is bimodal, i.e., the proton changes its position between O–H···O and O···H–O. The ReaxFF is designed to be capable of simulating chemical reactions including dissociation of molecules, and so, in principle, phases such as ice VII' may be observed under certain thermodynamic conditions; but in the region on the T, p plane examined in the present study, the bcc plastic ice phase is found to be stable on the high-pressure side of the domain of ice VII, and the proton translation disorder is not observed. In our preliminary *NpT* MD simulation with the ReaxFF potential, proton hopping or translation along between two neighboring oxygen atoms, which is associated with ice VII', is observed only at pressures and temperatures much higher than examined here, e.g., 170 GPa and 190 GPa at 1000 K and under 180 GPa at 850 K.

Finally, we shall compare the simulation results with the experimental results on dense ice. First, we note that no experimental studies so far report dense ice with the fcc structure in the pressure range examined here: recent work based on x-ray diffraction of shock-compressed water reports fcc ice above 100 GPa.⁴² The Raman

spectroscopy studies of dense ice by Pruzan *et al.*^{7,8} reported that the width of the ν_1 OH stretching mode as a function of pressure is minimal at around 12 GPa at room temperature. The non-monotonic behavior implies that the hydrogen bond in ice is strongest at that pressure and is notably weaker at pressures higher and lower than that point. Another experimental study shows evidence that ice VII contains hydrogen bonds with different lengths, indicating the structure of ice VII being more complex than previously thought.⁴³ A possible explanation, among many, is that the distribution in the hydrogen-bond length in ice VII is due to the distribution of molecular orientation in the predicted plastic ice. Recently, a time resolved x-ray diffraction study demonstrates that liquid water transforms to ice VII upon rapid compression, but whether that ice is crystalline or plastic remains undetermined.⁴⁴ The recent NMR study reports that chemical shift values in ice VII suggest two distinct transitions at 20 GPa and 75 GPa, the first one associated with some change in the character of hydrogen bonding in ice and the second one corresponding to the change from ice VII to ice X.¹⁵ It is unclear how the present results including the reentrant behavior of plastic phases are related to the experimental results. We note that the re-entrant behavior itself is not unique to the ReaxFF potential but is observed for the TIP4P/2005 model,³ however, it is not found by *ab initio* MD simulations.^{17–22}

IV. SUMMARY

The *NpT*-ensemble MD simulations with the ReaxFF potential were carried out to investigate high-pressure phase behavior of H₂O. Two stable plastic crystal phases having the fcc and bcc lattices were confirmed by the reorientational correlation function of H₂O molecules and the spatial distribution of protons.

The ReaxFF water exhibits VIII–VII and VII–fcc plastic phase changes as the temperature is increased at a fixed pressure of 8 GPa. VII-to-fcc plastic phase changes are observed with increasing temperature under 14 GPa or higher pressures and also observed with increasing pressure at 300 K. Fcc–bcc plastic phase changes are observed upon changing pressure at 450 K or higher temperatures.

A phase diagram derived from the ReaxFF MD simulations is given in Fig. 7. The fcc plastic phase lies on the low pressure side of ice VII and does the bcc plastic phase on the high pressure side. This feature is different from the results obtained from rigid models of water.³

The spatial distribution of protons in the fcc plastic crystal and that in the bcc plastic crystal are distinct from each other (see Fig. 3), reflecting different reorientational motions of H₂O molecules in the two plastic phases. In the fcc plastic ice, H₂O molecules rotate more or less freely, thereby having the distribution of a proton nearly uniform around an oxygen atom. On the other hand, in the bcc plastic phase, the distribution of each proton is annular around the axis connecting two oxygen atoms, as shown in Fig. 3(c), and it has a long tail when projected on that axis, as seen in Fig. 3(b). This means that water molecules undergo precession and occasionally rotate to change their hydrogen-bonding partners. The three kinds of characteristic rotational motions of H₂O molecules, “free” rotation in the lower-pressure fcc, “no” rotation in the middle-pressure ice VII, and “precessional” rotation in the higher-pressure bcc plastic phases,

are closely related to the longer, medium, and shorter distances d_{OO} between two neighboring oxygen atoms in the three phases.

Finally, it is, in principle, possible to observe rearrangement of chemical OH bonds and bimodal distributions of a proton between two oxygen atoms and thus a state called ice VII' in ReaxFF MD simulations; however, no such features are observed in the pressure and temperature ranges examined above: it is found from our preliminary NpT MD calculation that the ReaxFF H₂O ice does exhibit proton hopping or delocalization along between two neighboring oxygen atoms at 170 GPa, 1000 K and at 180 GPa, 850 K. The pressures and temperatures are higher than those at which delocalization is found by experiment and *ab initio* MD simulation. The discrepancy might suggest that the ReaxFF model of H₂O in the present form does not accurately reproduce the phase diagram involving superionic phases.

SUPPLEMENTARY MATERIAL

See the [supplementary material](#) for the diffusion coefficient data for the ReaxFF liquid water at high pressures and the radial distribution functions for the plastic ice phases.

ACKNOWLEDGMENTS

The authors are grateful to Professor T. C. Kobayashi for helpful discussions. This work was supported by the JSPS KAKENHI (Grant Nos. 26287099 and 18KK0151).

DATA AVAILABILITY

The data that support the findings of this study are available from the corresponding author upon reasonable request.

REFERENCES

- Y. Takii, K. Koga, and H. Tanaka, "A plastic phase of water from computer simulation," *J. Chem. Phys.* **128**, 204501–204508 (2008).
- J. L. Aragones, M. M. Conde, E. G. Noya, and C. Vega, "The phase diagram of water at high pressures as obtained by computer simulations of the TIP4P/2005 model: The appearance of a plastic crystal phase," *Phys. Chem. Chem. Phys.* **11**, 543–555 (2009).
- J. L. Aragones and C. Vega, "Plastic crystal phases of simple water models," *J. Chem. Phys.* **130**, 244504 (2009).
- K. Himoto, M. Matsumoto, and H. Tanaka, "Lattice- and network-structure in plastic ice," *Phys. Chem. Chem. Phys.* **13**, 19876–19881 (2011).
- K. Himoto, M. Matsumoto, and H. Tanaka, "Yet another criticality of water," *Phys. Chem. Chem. Phys.* **16**, 5081–5087 (2014).
- I. Skarmoutsos, S. Mossa, and E. Guardia, "The effect of polymorphism on the structural, dynamic and dielectric properties of plastic crystal water: A molecular dynamics simulation perspective," *J. Chem. Phys.* **150**, 124506–124515 (2019).
- P. Pruzan, J. C. Chervin, and M. Gauthier, "Raman spectroscopy investigation of ice VII and deuterated ice VII to 40 GPa disorder in ice VII," *Europhys. Lett.* **13**, 81–87 (1990).
- P. Pruzan, J. C. Chervin, E. Wolanin, B. Canny, M. Gauthier, and M. Hanfland, "Phase diagram of ice in the VII–VIII–X domain. Vibrational and structural data for strongly compressed ice VIII," *J. Raman Spectrosc.* **34**, 591–610 (2003).
- N. Noguchi and T. Okuchi, "Self-diffusion of protons in H₂O ice VII at high pressures: Anomaly around 10 GPa," *J. Chem. Phys.* **144**, 234503–234510 (2016).
- C.-S. Zha, J. S. Tse, and W. A. Bassett, "New Raman measurements for H₂O ice VII in the range of 300 cm⁻¹ to 4000 cm⁻¹ at pressures up to 120 GPa," *J. Chem. Phys.* **145**, 124315–124319 (2016).
- M. Somayazulu, J. Shu, C.-S. Zha, A. F. Goncharov, O. Tschauner, H.-k. Mao, and R. J. Hemley, "In situ high-pressure x-ray diffraction study of H₂O ice VII," *J. Chem. Phys.* **128**, 064510–064511 (2008).
- H. Kadobayashi, H. Hirai, T. Matsuoka, Y. Ohishi, and Y. Yamamoto, "A possible existence of phase change of deuterated ice VII at about 11 GPa by X-ray and Raman studies," *J. Phys.: Conf. Ser.* **500**, 182017–1–182017–6 (2014).
- M. Guthrie, R. Boehler, C. A. Tulk, J. J. Molaison, A. M. dos Santos, K. Li, and R. J. Hemley, "Neutron diffraction observations of interstitial protons in dense ice," *Proc. Natl. Acad. Sci. U. S. A.* **110**, 10552–10556 (2013).
- M. Guthrie, R. Boehler, J. J. Molaison, B. Haberl, A. M. dos Santos, and C. Tulk, "Structure and disorder in ice VII on the approach to hydrogen-bond symmetrization," *Phys. Rev. B* **99**, 184112 (2019).
- T. Meier, S. Petitgirard, S. Khandarkhaeva, and L. Dubrovinsky, "Observation of nuclear quantum effects and hydrogen bond symmetrisation in high pressure ice," *Nat. Commun.* **9**, 2766–1–2766–7 (2018).
- K. Mochizuki, K. Himoto, and M. Matsumoto, "Diversity of transition pathways in the course of crystallization into ice VII," *Phys. Chem. Chem. Phys.* **16**, 16419–16425 (2014).
- M. Benoit, D. Marx, and M. Parrinello, "Tunnelling and zero-point motion in high-pressure ice," *Nature* **392**, 258–261 (1998).
- M. Benoit, A. H. Romero, and D. Marx, "Reassigning hydrogen-bond centering in dense ice," *Phys. Rev. Lett.* **89**, 145501 (2002).
- J. A. Morrone, L. Lin, and R. Car, "Tunneling and delocalization effects in hydrogen bonded systems: A study in position and momentum space," *J. Chem. Phys.* **130**, 204511–204514 (2009).
- J.-A. Hernandez and R. Caracas, "Superionic-superionic phase transitions in body-centered cubic H₂O ice," *Phys. Rev. Lett.* **117**, 135503 (2016).
- Z. Futera and N. J. English, "Pressure dependence of structural properties of ice VII: An *ab initio* molecular-dynamics study," *J. Chem. Phys.* **148**, 204505 (2018).
- T. Ikeda, "First principles centroid molecular dynamics simulation of high pressure ices," *J. Chem. Phys.* **148**, 102332–102339 (2018).
- J.-A. Hernandez and R. Caracas, "Proton dynamics and the phase diagram of dense water ice," *J. Chem. Phys.* **148**, 214501–214512 (2018).
- A. C. T. van Duin, S. Dasgupta, F. Lorant, and W. A. Goddard, "ReaxFF: A reactive force field for hydrocarbons," *J. Phys. Chem. A* **105**, 9396–9409 (2001).
- T. P. Senftle, S. Hong, M. M. Islam, S. B. Klyasa, Y. R. Engel-Herbert, M. J. Janik, H. M. Aktulga, T. Verstraelen, A. Grama, and A. C. T. van Duin, "The ReaxFF reactive force-field: Development, applications and future directions," *npj Comput. Mater.* **2**, 15011 (2016).
- O. Rahaman, A. C. T. van Duin, W. A. Goddard III, and D. J. Doren, "Development of a ReaxFF reactive force field for glycine and application to solvent effect and tautomerization," *J. Phys. Chem. B* **115**, 249–261 (2011).
- J. C. Fogarty, H. M. Aktulga, A. Y. Grama, A. C. T. van Duin, and S. A. Pandit, "A reactive molecular dynamics simulation of the silica-water interface," *J. Chem. Phys.* **132**, 174704–174711 (2010).
- M. Sobrino Fernandez Mario, M. Neek-Amal, and F. M. Peeters, "AA-stacked bilayer square ice between graphene layers," *Phys. Rev. B* **92**, 245428–1–245428–5 (2015).
- V. Satarifard, M. Mousaei, F. Hadadi, J. Dix, M. S. Fernandez, P. Carbone, J. Beheshtian, F. M. Peeters, and M. Neek-Amal, "Reversible structural transition in nanoconfined ice," *Phys. Rev. B* **95**, 064105 (2017).
- M. Raju, A. Duin, and M. Ihme, "Phase transitions of ordered ice in graphene nanocapillaries and carbon nanotubes," *Sci. Rep.* **8**, 3851 (2018).
- K. Koga, G. T. Gao, H. Tanaka, and X. C. Zeng, "Formation of ordered ice nanotubes inside carbon nanotubes," *Nature* **412**, 802–805 (2001).
- K. Koga, X. C. Zeng, and H. Tanaka, "Freezing of confined water: A bilayer ice phase in hydrophobic nanopores," *Phys. Rev. Lett.* **79**, 5262 (1997).

- ³³R. Zangi and A. E. Mark, "Monolayer ice," *Phys. Rev. Lett.* **91**, 025502–025504 (2003).
- ³⁴Y. Maniwa, H. Kataura, M. Abe, S. Suzuki, Y. Achiba, H. Kira, and K. Matsuda, "Phase transition in confined water inside carbon nanotubes," *J. Phys. Soc. Jpn.* **71**, 2863–2866 (2002).
- ³⁵G. Algara-Siller, O. Lehtinen, F. C. Wang, R. R. Nair, U. Kaiser, H. A. Wu, A. K. Geim, and I. V. Grigorieva, "Square ice in graphene nanocapillaries," *Nature* **519**, 443–445 (2015).
- ³⁶S. Plimpton, "Fast parallel algorithms for short-range molecular dynamics," *J. Comput. Phys.* **117**, 1–19 (1995).
- ³⁷K. Koga and H. Tanaka, "Rearrangement dynamics of the hydrogen-bonded network of clathrate hydrates encaging polar guest," *J. Chem. Phys.* **104**, 263 (1996).
- ³⁸I. Ohmine and H. Tanaka, "Fluctuation, relaxations, and hydration in liquid water. Hydrogen-bond rearrangement dynamics," *Chem. Rev.* **93**, 2545–2566 (1993).
- ³⁹M. G. Mazza, N. Giovambattista, H. E. Stanley, and F. W. Starr, "Connection of translational and rotational dynamical heterogeneities with the breakdown of the Stokes-Einstein and Stokes-Einstein-Debye relations in water," *Phys. Rev. E* **76**, 031203 (2007).
- ⁴⁰L. E. Bove, S. Klotz, T. Strässle, M. Koza, J. Teixeira, and A. M. Saitta, "Translational and rotational diffusion in water in the gigapascal range," *Phys. Rev. Lett.* **111**, 185901–185905 (2013).
- ⁴¹M. French, M. P. Desjarlais, and R. Redmer, "Ab initio calculation of thermodynamic potentials and entropies for superionic water," *Phys. Rev. E* **93**, 022140-1–022140-11 (2016).
- ⁴²M. Millot, F. Coppari, J. R. Rygg, A. Correa Barrios, S. Hamel, D. C. Swift, and J. H. Eggert, "Nanosecond X-ray diffraction of shock-compressed superionic water ice," *Nature* **569**, 251–255 (2019).
- ⁴³R. J. Nelmes, J. S. Loveday, W. G. Marshall, G. Hamel, J. M. Besson, and S. Klotz, "Multisite disordered structure of ice VII to 20 GPa," *Phys. Rev. Lett.* **81**, 2719–2722 (1998).
- ⁴⁴A. E. Gleason, C. A. Bolme, E. Galtier, H. J. Lee, E. Granados, D. H. Dolan, C. T. Seagle, T. Ao, S. Ali, A. Lazicki, D. Swift, P. Celliers, and W. L. Mao, "Compression freezing kinetics of water to ice VII," *Phys. Rev. Lett.* **119**, 025701 (2017).